


## Method and computer library for calculation of the Boltzmann collision integrals on discrete momentum lattice

I. O. Kuznetsov  and P. F. Kartsev \*

*National Research Nuclear University MEPhI (Moscow Engineering Physics Institute), 115409 Moscow, Russia*

 (Received 1 December 2020; revised 1 September 2022; accepted 4 April 2023; published 11 May 2023)

We present a general and numerically efficient method for calculation of collision integrals for interacting quantum gases on a discrete momentum lattice. Here we employ the original analytical approach based on Fourier transform covering a wide spectrum of solid-state problems with various particle statistics and arbitrary interaction models, including the case of momentum-dependent interaction. The comprehensive set of the transformation principles is given in detail and realized as a computer Fortran 90 library FLBE (Fast Library for Boltzmann Equation).

DOI: [10.1103/PhysRevE.107.055304](https://doi.org/10.1103/PhysRevE.107.055304)

### I. INTRODUCTION

Recent advances of experimental physics in generation of ultrashort laser pulses, including attosecond duration [1,2], present the possibility to obtain and study nonequilibrium states of matter with femtosecond [3–5] and even attosecond [6] resolution. The details of relaxation processes in the excited state allows us to clarify the material characteristics [3] or interaction models [4], and help to develop unique optoelectronic devices [7,8].

There exist many theoretical approaches, such as Liouville equation [9], nonequilibrium Green's function method [10–14], real-time density functional theory [15], and others [16], developed to describe nonequilibrium phenomena in various physical models.

In the case of the solid state, the excited state quickly becomes near equilibrium due to high collision rate in the condensed state. As a result, the system behavior can be efficiently described by the kinetic Boltzmann equation [17,18] in the whole time range of consideration, including femtosecond scale [19–22]. On the other side, in the case of shorter times, higher excitation levels or significant correlations between particles, accurate consideration can require the application of more advanced approaches [23] listed above.

Overall, the kinetic Boltzmann equation provides a simple and clear description for the behavior of statistical systems in the language of the time-dependent particle distribution function. Interparticle interaction enters the equation in the form of collision integrals which are based on the interaction type and particle statistics. In calculation of collision integrals, various simplifications are often used, e.g., averaging the distribution over the direction of momentum [19]. Reformulation of the equation to the integral features of the distribution function, such as particle density, temperature, or total energy, resulted in many useful and practical models, such as the relaxation-time approximation [5], Rothwarf-Taylor [24–26],

and the two-temperature [15,21] or three-temperature model [27]. Still, the original form of the Boltzmann equation, taking into account actual momentum distribution, gives more information and research possibilities [22].

In this paper, we present the general and numerically efficient method for calculation of collision integrals for a wide spectrum of solid-state problems with various particle statistics and arbitrary interaction models.

The paper is organized as follows. First, we show the main idea of the approach on the example of a Hubbard-like model using the convolution structure of the collision integrals, allowing us to accelerate the calculation using the Fourier transform (Sec. II). In Sec. III, the relations are generalized to the case of an arbitrary nonequidistant energy spectrum with introduction of the level broadening factor and appropriate selection of energy axis discretization. Next, we make use of the universal structure of the formula (Secs. IV–VI), allowing us to apply the transformation to other interaction types, such as electron-phonon, etc., including the case of momentum-dependent matrix elements, and calculate the linear response coefficients.

The comprehensive set of transformation rules for collision integrals and linear response coefficients was realized in the form of a computer library. In Sec. VII, we present the main facts and performance benchmarks for the library. In Sec. VIII, we demonstrate the application of the approach to the study of nonequilibrium state relaxation in three problems of condensed matter physics.

### II. FREE GAS WITH MOMENTUM-INDEPENDENT INTERACTION

In this section, we start with the simplest case of free gas with momentum-independent interaction constant  $U_{\mathbf{q}} = \text{const} = U_0$  to demonstrate the main principles of the transformation.

The Hamiltonian of the system has the form

$$\hat{H} = \hat{H}_0 + \hat{H}_{\text{int}}, \quad (1)$$

\*Corresponding author: [petr.f.kartsev@gmail.com](mailto:petr.f.kartsev@gmail.com)

where  $\hat{H}_0$  and  $\hat{H}_{\text{int}}$  are the single-particle Hamiltonian and interaction part, correspondingly,

$$\hat{H}_0 = \sum_{\mathbf{k}} \varepsilon_{\mathbf{k}} \hat{n}_{\mathbf{k}} = \varepsilon_1 \sum_{\mathbf{k}} \mathbf{k}^2 \hat{n}_{\mathbf{k}}, \quad (2)$$

where  $\varepsilon_{\mathbf{k}} \sim \mathbf{k}^2$  is the kinetic energy of free particles and  $\hat{n}_{\mathbf{k}}$  is the operator of occupation number.

The interaction term is taken in the simplest form of the Hubbard model for Fermi system, and Bose-Hubbard for Bose system, respectively,

$$\hat{H}_{\text{int}}^{(F)} = U \sum_{\mathbf{i}} \hat{n}_{\mathbf{i}\uparrow} \hat{n}_{\mathbf{i}\downarrow}, \quad (3)$$

$$\hat{H}_{\text{int}}^{(B)} = U \sum_{\mathbf{i}} \hat{n}_{\mathbf{i}} (\hat{n}_{\mathbf{i}} - 1), \quad (4)$$

where the summation goes over the sites  $\mathbf{i}$  of a finite atomic cluster or nanocrystal containing  $L \times L \times L$  atoms with periodic boundary conditions.

After conversion to momentum space, both Eqs. (3) and (4) obtain the form

$$\hat{H}_{\text{int}} = U_0 \sum_{1234} \hat{a}_1^\dagger \hat{a}_2^\dagger \hat{a}_3 \hat{a}_4 \delta_{1+2,3+4+\mathbf{G}}, \quad (5)$$

where we introduced the parameter  $U_0 \equiv U/L^3$ . For the purposes of the following discussion, we denote the momenta of four particles involved in the interaction  $\mathbf{k}$ ,  $\mathbf{p}$ ,  $\mathbf{p} + \mathbf{q}$ ,  $\mathbf{k} - \mathbf{q}$  as **1**, **2**, **3**, **4**, correspondingly, and the conservation law is shown explicitly with Kronecker delta. Later, the reciprocal lattice vector  $\mathbf{G}$  is assumed and not shown for simplicity.

The discrete momentum lattice takes the form of a Monkhorst-Pack grid with  $L \times L \times L$  points covering the first Brillouin zone; the momentum step is  $\Delta k = 2\pi/La$ , with  $a$  the lattice constant. Similar discretization can be used for larger volumes of the crystal provided that the particle distribution function is smooth enough in the momentum space.

Taking into account relatively small dimensions of the system, we assume that the particle distribution function is homogeneous in space and depends only on time and momentum coordinates  $\{n_{\mathbf{k}}(t)\}$ . In this case, the kinetics of the system is described by the Boltzmann equation without the diffusion term [19],

$$\frac{dn_{\mathbf{k}}}{dt} = J_{\mathbf{k}}, \quad (6)$$

where  $J_{\mathbf{k}}$  are the collision integrals having the following form:

$$J_{1\sigma} = U_0^2 \sum_{234} [(1 - n_{1\sigma})(1 - n_{2\bar{\sigma}})n_{3\bar{\sigma}}n_{4\sigma} - n_{1\sigma}n_{2\bar{\sigma}}(1 - n_{3\bar{\sigma}})(1 - n_{4\sigma})] \delta_{\Delta\varepsilon,0} \delta_{1+2,3+4} \quad (7)$$

for Fermi statistics and

$$J_1 = 2U_0^2 \sum_{234} [(n_1 + 1)(n_2 + 1 + \delta_{12})n_3(n_4 - \delta_{34}) - n_1(n_2 - \delta_{12})(n_3 + 1)(n_4 + 1 + \delta_{34})] \delta_{\Delta\varepsilon,0} \delta_{1+2,3+4} \quad (8)$$

for Bose statistics, respectively. Note the corrections using  $\delta_{12}$ ,  $\delta_{34}$  in the terms with coinciding states. While they are negligible in the continual case, for a finite system the exact

form is essential. For simplicity, we use the time units where  $2\pi/\hbar = 1$ .

The application of the Boltzmann equation to continual problems often comes down to performing integration with energy-dependent functions [19,23]. This approach ignores the details of momentum distribution which can be essential for the nonequilibrium state. To take into account the actual momentum distribution, the numerical summation of the original expressions on a discrete momentum lattice is preferable. On the other side, the number of terms in this case rapidly grows with the lattice size  $L$  as  $\sim L^9$ , motivating the application of high-performance and supercomputing technologies [28,29]. In this section, we demonstrate the main principles of the transformation, allowing us to decrease the scaling index and, respectively, expand the affordable system size range. Let us expand the brackets in Eq. (8) and group the terms:

$$J_1 = 2U_0^2 \sum_{234} \{ [n_2 n_3 n_4 + n_3 n_4 + n_1 \times (n_3 n_4 - n_2 n_3 - n_2 n_4 - n_2)] - \delta_{34} [(n_2 n_3 + n_3) + n_1 (2n_2 n_3 + n_2 + n_3)] + \delta_{12} [n_3 n_4 + n_1 (2n_3 n_4 + n_3 + n_4 + 1)] + \delta_{12} \delta_{34} (n_1 - n_3) \} \delta_{\varepsilon_1 + \varepsilon_2, \varepsilon_3 + \varepsilon_4} \delta_{1+2,3+4}. \quad (9)$$

First, we note that due to momentum conservation  $\delta_{1+2,3+4}$ , all terms in (9) have the form of a discrete convolution of periodic functions in  $\mathbf{k}$  space,

$$\sum_{\mathbf{k}'} x(\mathbf{k}') y(\mathbf{k} - \mathbf{k}') \equiv (x * y)(\mathbf{k}), \quad (10)$$

which can be efficiently calculated using the convolution theorem,

$$(x * y)(\mathbf{k}) = \mathcal{F}^{-1} [X(\mathbf{r}) \cdot Y(\mathbf{r})](\mathbf{k}), \quad (11)$$

where symbols  $\mathcal{F}$ ,  $\mathcal{F}^{-1}$  denote the forward and backward Fourier transforms:

$$X(\mathbf{r}) = \mathcal{F} [x(\mathbf{k})] \equiv \sum_{\mathbf{k}} x(\mathbf{k}) e^{-i\mathbf{k}\mathbf{r}},$$

$$x(\mathbf{k}) = \mathcal{F}^{-1} [X(\mathbf{r})] \equiv \frac{1}{L^3} \sum_{\mathbf{r}} X(\mathbf{r}) e^{i\mathbf{k}\mathbf{r}}.$$

This allows us to calculate the sum (10) with  $\sim L^3 \ln L$  operations using the fast Fourier transform (FFT).

The same transformation can be performed on the energy axis [28,30], since the discrete particle energies in this model are proportional to integer numbers:  $\varepsilon_n = n\varepsilon_1$ , where  $n = 0 \dots N_\varepsilon - 1$ . To use this scheme correctly for functions without periodicity on the energy axis, the extended range of values  $n = 0 \dots N_{\text{max}} - 1$  is employed, with the so-called zero-padding [31] at  $n \geq N_\varepsilon$ .

Finally, we introduce the functions in the extended 4D space  $(\mathbf{k}, \varepsilon) \equiv \kappa$  and  $(\mathbf{r}, \gamma) \equiv \mathbf{R}$ :

$$n_{\mathbf{k}\varepsilon} \equiv n_{\mathbf{k}} \delta_{\varepsilon, \varepsilon_{\mathbf{k}}}, \quad (12)$$

$$s_{\mathbf{k}\varepsilon} \equiv \delta_{\varepsilon, \varepsilon_{\mathbf{k}}}, \quad (13)$$

$$N_{\mathbf{R}} \equiv \mathcal{F}(n_{\kappa}), \quad (14)$$

$$S_{\mathbf{R}} \equiv \mathcal{F}(s_{\kappa}). \quad (15)$$

Using Eqs. (12)–(15) in the expressions (7) and (8) and replacing the respective Kronecker delta with sums  $\delta_{\mathbf{k},\mathbf{k}'} = \frac{1}{L^3} \sum_{\mathbf{r}} e^{i(\mathbf{k}-\mathbf{k}')\mathbf{r}}$  and  $\delta_{\varepsilon,\varepsilon'} = \frac{1}{N_\varepsilon} \sum_{\gamma} e^{i(\varepsilon-\varepsilon')\gamma}$ , we obtain the resulting relation:

$$J_{\mathbf{k}} = U_0^2 [(p_{\mathbf{k},\varepsilon_{\mathbf{k}}} + \tilde{p}_{2\mathbf{k},2\varepsilon_{\mathbf{k}}}) + n_{\mathbf{k}}(q_{\mathbf{k},\varepsilon_{\mathbf{k}}} + \tilde{q}_{2\mathbf{k},2\varepsilon_{\mathbf{k}}})]. \quad (16)$$

Here we introduced the following notations:

$$\begin{aligned} p_{\kappa} &\equiv \mathcal{F}^{-1}(P_{\mathbf{R}}), \\ q_{\kappa} &\equiv \mathcal{F}^{-1}(Q_{\mathbf{R}}), \\ \tilde{p}_{\kappa} &\equiv \mathcal{F}^{-1}(\tilde{P}_{\mathbf{R}}), \\ \tilde{q}_{\kappa} &\equiv \mathcal{F}^{-1}(\tilde{Q}_{\mathbf{R}}), \end{aligned} \quad (17)$$

where

$$\begin{aligned} P_{\mathbf{R}} &= 2(S_{-\mathbf{R}}N_{\mathbf{R}}^2 + N_{-\mathbf{R}}N_{\mathbf{R}}^2 - N_{-\mathbf{R}}N_{2\mathbf{R}} - S_{-\mathbf{R}}N_{2\mathbf{R}}), \\ \tilde{P}_{\mathbf{R}} &= 2N_{\mathbf{R}}^2 - N_{2\mathbf{R}}, \\ Q_{\mathbf{R}} &= 2(S_{-\mathbf{R}}n_{\mathbf{R}}^2 - 2N_{-\mathbf{R}}N_{\mathbf{R}}S_{\mathbf{R}} - N_{-\mathbf{R}}S_{\mathbf{R}}^2 - N_{-\mathbf{R}}S_{2\mathbf{R}} \\ &\quad - S_{-\mathbf{R}}N_{2\mathbf{R}} - 2N_{-\mathbf{R}}N_{2\mathbf{R}}), \\ \tilde{Q}_{\mathbf{R}} &= 2(S_{\mathbf{R}}^2 + 2N_{\mathbf{R}}S_{\mathbf{R}} + 2N_{\mathbf{R}}^2 + S_{2\mathbf{R}}) \end{aligned} \quad (18)$$

in the case of Bose statistics, and

$$\begin{aligned} P_{\mathbf{R}} &= S_{-\mathbf{R}}N_{\mathbf{R}}^2 - N_{-\mathbf{R}}N_{\mathbf{R}}^2 + N_{-\mathbf{R}}N_{2\mathbf{R}} - S_{-\mathbf{R}}N_{2\mathbf{R}}, \\ \tilde{P}_{\mathbf{R}} &= -N_{\mathbf{R}}^2 + N_{2\mathbf{R}}, \\ Q_{\mathbf{R}} &= -S_{-\mathbf{R}}N_{\mathbf{R}}^2 + 2N_{-\mathbf{R}}N_{\mathbf{R}}S_{\mathbf{R}} - N_{-\mathbf{R}}S_{\mathbf{R}}^2 \\ &\quad + N_{-\mathbf{R}}S_{2\mathbf{R}} + S_{-\mathbf{R}}N_{2\mathbf{R}} - 2N_{-\mathbf{R}}N_{2\mathbf{R}}, \\ \tilde{Q}_{\mathbf{R}} &= S_{\mathbf{R}}^2 - 2N_{\mathbf{R}}S_{\mathbf{R}} + 2N_{\mathbf{R}}^2 - S_{2\mathbf{R}} \end{aligned} \quad (19)$$

in the case of Fermi statistics (paying additional attention to spin indexes). The detailed derivation is given in the Appendix.

In conclusion, multiple sums in the expressions (7) and (8) are converted to the chain of several Fourier transforms which are more performance-efficient [10]. The amount of calculations can be estimated as  $\sim L^5 \ln L$  due to  $N_\varepsilon \sim L^2$ . This makes it possible to increase the size of the system to a relatively macroscopic  $L \sim 16 \div 64$ , depending on the available computing resources, and approach the continual limit. Several works dealing with similar grid sizes  $L \sim 40 \div 50$  for the numerical solution of the Kadanoff-Baym equations use similar FFT-based approaches [32–34].

### III. ENERGY LEVEL BROADENING AND ARBITRARY SPECTRUM

To take into account the finite linewidth of the energy levels, we replace  $\delta_{\Delta\varepsilon,0}$  with broadening factor  $f(\Delta\varepsilon)$ :

$$\sum_{\substack{\mathbf{k}_2 \mathbf{k}_3 \mathbf{k}_4 \\ \varepsilon_2 \varepsilon_3 \varepsilon_4}} (\dots) \delta_{\Delta\varepsilon,0} \rightarrow \sum_{\substack{\mathbf{k}_2 \mathbf{k}_3 \mathbf{k}_4 \\ \varepsilon_2 \varepsilon_3 \varepsilon_4}} (\dots) f(\Delta\varepsilon). \quad (20)$$

As a result, the expressions in (17) become

$$\begin{aligned} p_{\mathbf{k}\varepsilon} &\equiv \mathcal{F}^{-1}(P_{\mathbf{r}\gamma} F(\gamma)), \\ q_{\mathbf{k}\varepsilon} &\equiv \mathcal{F}^{-1}(Q_{\mathbf{r}\gamma} F(\gamma)), \\ \tilde{p}_{\mathbf{k}\varepsilon} &\equiv \mathcal{F}^{-1}(\tilde{P}_{\mathbf{r}\gamma} F(\gamma)), \\ \tilde{q}_{\mathbf{k}\varepsilon} &\equiv \mathcal{F}^{-1}(\tilde{Q}_{\mathbf{r}\gamma} F(\gamma)), \end{aligned} \quad (21)$$

where  $F(\gamma)$  is the Fourier transform of the factor  $f(\varepsilon)$ .

The same approach allows us to take into account arbitrary energy levels  $\varepsilon_{\mathbf{k}}$ , i.e., for systems with nonparabolic dispersion law (acoustic phonons, exciton polaritons, Bogoliubov quasiparticles in superconductors, etc.).

In the case when the energy levels are not equidistant, discrete Fourier transform on an energy axis involves rounding to the evenly distributed values, leading to the loss of calculation precision. With a smaller step on the energy axis, we can make the grid values closer to the actual single-particle energy levels. Note that in the case of the problem with several interaction terms in the Hamiltonian or particle sorts—e.g., electrons and holes—each term in the collision integral may require different energy discretization steps.

The necessary accuracy of the approximation is determined by the width of the levels in the physical problem, as well as the broadening factor  $f(\Delta\varepsilon)$ , which can be taken in the form of Lorentzian or Gaussian function, depending on the problem under consideration [35].

The introduction of the broadening factor along with the reasonable choice of smaller energy step allows us to consider systems with arbitrary not equidistant single-particle spectrums.

### IV. UNIVERSAL REPRESENTATION

Now we develop the demonstrated approach to the general set of rules allowing effective calculation of collision integrals for any interaction type.

Indeed, the terms in Eq. (9) can be represented in the universal form not specific to the pair interaction, namely, the first line can be written as

$$J_{\mathbf{k}}^{(1)} = \sum_{\nu} K_{\nu} A_{\mathbf{k}}^{(\nu)} w_{\mathbf{k}}^{(\nu)}, \quad (22)$$

where  $K_{\nu}$  are the coefficients,  $\nu$  denotes the terms from the set (A3)–(A6),

$$w_{\mathbf{1}}^{(\nu)} = \sum_{234} B_2^{(\nu)} C_3^{(\nu)} D_4^{(\nu)} \delta_{\mathbf{1}+\mathbf{2},\mathbf{3}+\mathbf{4}} f(\Delta\varepsilon), \quad (23)$$

the factors  $A_{\mathbf{k}}, \dots, D_{\mathbf{k}}$  are equal to  $n_{\mathbf{k}}$  or unity for the corresponding term, and  $\Delta\varepsilon \equiv \varepsilon_1 + \varepsilon_2 - \varepsilon_3 - \varepsilon_4$ . Then, repeating the conversion from the Appendix and paying attention to the corresponding indexes, we arrive at

$$w_{\mathbf{k}}^{(\nu)} = \mathcal{F}_{\mathbf{k},\varepsilon_{\mathbf{k}}}^{-1} \{ B_{-\mathbf{R}}^{(\nu)} C_{\mathbf{R}}^{(\nu)} D_{\mathbf{R}}^{(\nu)} F(\gamma) \}. \quad (24)$$

Here the indexes of factors  $B, C, D$  have a sign which is determined by the position of the respective momentum in the conservation law, i.e., the type of the particle operator—creation or annihilation—in the interaction term.

Next we discuss the terms with Kronecker delta. The term with  $\delta_{34}$  gives the components (A14)–(A16),

$$x_{\mathbf{1}}^{(v)} = \sum_{234} B_2^{(v)} C_3^{(v)} \delta_{34} \delta_{1+2,3+4} f(\Delta\varepsilon), \quad (25)$$

which transform to

$$x_{\mathbf{k}}^{(v)} = \mathcal{F}_{\mathbf{k},\varepsilon_{\mathbf{k}}}^{-1} \{B_{-\mathbf{R}}^{(v)} C_{2\mathbf{R}}^{(v)} F(\gamma)\}, \quad (26)$$

while the components (A21)–(A23) for  $\delta_{12}$  transform to

$$y_{\mathbf{k}}^{(v)} = \mathcal{F}_{2\mathbf{k},2\varepsilon_{\mathbf{k}}}^{-1} \{C_{\mathbf{R}}^{(v)} D_{\mathbf{R}}^{(v)} F(\gamma)\}, \quad (27)$$

and finally the term (A28) for  $\delta_{12}\delta_{34}$  gives

$$z_{\mathbf{k}}^{(v)} = \mathcal{F}_{2\mathbf{k},2\varepsilon_{\mathbf{k}}}^{-1} \{C_{2\mathbf{R}}^{(v)} F(\gamma)\}. \quad (28)$$

As we see, the presence of the Kronecker delta results in the multipliers at the corresponding indexes, namely, at  $\kappa \equiv (\mathbf{k}, \varepsilon_{\mathbf{k}})$  for  $\delta_{12}$  and  $\mathbf{R} \equiv (\mathbf{r}, \gamma)$  for  $\delta_{34}$ .

Such representation in  $A/B/C/D$  form is not limited to pair interaction. For instance, the electron-phonon interaction

$$\hat{H}^{(e-ph)} = M_0 \sum_{\mathbf{k}\mathbf{q}\sigma} \hat{a}_{\mathbf{k}\sigma}^\dagger \hat{a}_{\mathbf{k}-\mathbf{q},\sigma} (\hat{b}_{\mathbf{q}}^\dagger + \hat{b}_{-\mathbf{q}}) \quad (29)$$

gives the collision integrals

$$J_{\mathbf{k}_1\sigma}^{(a)} = M_0^2 \sum_{\mathbf{k}_2\mathbf{q}} \{ [(1 - n_{\mathbf{k}_1\sigma}^{(a)}) (n_{\mathbf{q}}^{(b)} + 1) n_{\mathbf{k}_2\sigma}^{(a)} - n_{\mathbf{k}_1\sigma}^{(a)} n_{\mathbf{q}}^{(b)} (1 - n_{\mathbf{k}_2\sigma}^{(a)})] \delta_{\mathbf{k}_1+\mathbf{q},\mathbf{k}_2} f(\varepsilon_{\mathbf{k}_1}^{(a)} + \varepsilon_{\mathbf{q}}^{(b)} - \varepsilon_{\mathbf{k}_2}^{(a)}) + [(1 - n_{\mathbf{k}_1\sigma}^{(a)}) n_{\mathbf{q}}^{(b)} n_{\mathbf{k}_2\sigma}^{(a)} - n_{\mathbf{k}_1\sigma}^{(a)} (n_{\mathbf{q}}^{(b)} + 1) (1 - n_{\mathbf{k}_2\sigma}^{(a)})] \delta_{\mathbf{k}_1-\mathbf{q},\mathbf{k}_2} f(\varepsilon_{\mathbf{k}_1}^{(a)} - \varepsilon_{\mathbf{q}}^{(b)} - \varepsilon_{\mathbf{k}_2}^{(a)}) \}, \quad (30)$$

$$J_{\mathbf{q}}^{(b)} = M_0^2 \sum_{\mathbf{k}_1\mathbf{k}_2\sigma} [(1 - n_{\mathbf{k}_1\sigma}^{(a)}) (n_{\mathbf{q}}^{(b)} + 1) n_{\mathbf{k}_2\sigma}^{(a)} - n_{\mathbf{k}_1\sigma}^{(a)} n_{\mathbf{q}}^{(b)} (1 - n_{\mathbf{k}_2\sigma}^{(a)})] \delta_{\mathbf{k}_1+\mathbf{q},\mathbf{k}_2} f(\varepsilon_{\mathbf{k}_1}^{(a)} + \varepsilon_{\mathbf{q}}^{(b)} - \varepsilon_{\mathbf{k}_2}^{(a)}), \quad (31)$$

where the respective electron and phonon terms are indicated by  $a$  and  $b$ . As we see, the expressions (30) and (31) have the form (22) with the components

$$w_{\mathbf{k}}^{(v)} = \mathcal{F}_{\mathbf{k},\varepsilon_{\mathbf{k}}}^{-1} \{B_{-\mathbf{R}}^{(v)} C_{\mathbf{R}}^{(v)} F(\gamma)\},$$

compatible with the general approach discussed above.

Similarly, this set of rules can be used when the perturbation consists of more than four operators. For instance, the hypothetical interaction with five operators

$$\hat{H}_5 = V \sum_{12345} \hat{a}_1^\dagger \hat{a}_2^\dagger \hat{a}_3 \hat{a}_4 \hat{a}_5 \delta_{1+2,3+4+5} \quad (32)$$

gives the following components of collision integrals:

$$w_{\mathbf{1}}^{(v)} = \sum_{2345} B_2^{(v)} C_3^{(v)} D_4^{(v)} E_5^{(v)} \delta_{1+2,3+4+5} f(\Delta\varepsilon), \quad (33)$$

transforming to

$$w_{\mathbf{k}}^{(v)} = \mathcal{F}_{\mathbf{k},\varepsilon_{\mathbf{k}}}^{-1} \{B_{-\mathbf{R}}^{(v)} C_{\mathbf{R}}^{(v)} D_{\mathbf{R}}^{(v)} E_{\mathbf{R}}^{(v)} F(\gamma)\}. \quad (34)$$

The components with Kronecker delta, for example,  $\delta_{12}\delta_{34}\delta_{45}$ , give

$$w_{\mathbf{1}}^{(v)} = \sum_{2345} \delta_{12} C_3^{(v)} \delta_{34} \delta_{45} \delta_{1+2,3+4+5} f(\Delta\varepsilon), \quad (35)$$

which transforms to

$$w_{\mathbf{k}}^{(v)} = \mathcal{F}_{2\mathbf{k},2\varepsilon_{\mathbf{k}}}^{-1} \{C_{3\mathbf{R}}^{(v)} F(\gamma)\}, \quad (36)$$

obeying the same principles.

As a conclusion, the general set of rules discussed in this section allows us to use the FFT-accelerated approach to calculate the collision integrals for a wide range of interaction types.

We should mention, however, that this representation can be suboptimal when the interaction is simple enough. Indeed, in the case of electron-phonon interaction with three operators (29), there are not many combinations of momenta  $\{\mathbf{k}_1, \mathbf{q}\}$  giving nonzero terms in the collision integrals. As a result,

all combinations can be determined and tabulated in advance, giving a calculation complexity as low as  $\sim L^3$ .

## V. LINEAR RESPONSE COEFFICIENTS

The same approach can be used to calculate the linear response coefficients which describe the change of collision integrals due to small perturbations of the distribution function.

For the occupation numbers close to equilibrium distribution where  $J_{\mathbf{k}}^{(0)} = 0$ , Boltzmann equation can be linearized to give the so-called relaxation-time approximation [17,18,36,37]:

$$n_{\mathbf{k}} = n_{\mathbf{k}}^{(0)} + \delta n_{\mathbf{k}} \rightarrow J_{\mathbf{k}} = J_{\mathbf{k}}^{(0)} + \delta J_{\mathbf{k}}, \quad (37)$$

$$\frac{dn_{\mathbf{k}}}{dt} = \delta J_{\mathbf{k}} \simeq -\frac{n_{\mathbf{k}} - n_{\mathbf{k}}^{(0)}}{\tau_{\mathbf{k}}}. \quad (38)$$

Note that the linearization of relations (7) and (8) keeps the general form shown in Sec. IV which allows us to apply the transformation. Indeed, let us differentiate Eq. (7) by  $n_{1\sigma}$ :

$$\begin{aligned} \frac{\partial J_{\mathbf{1}}}{\partial n_{1\sigma}} &= U_0^2 \sum_{234} \{ (-1)(1 - n_{2\bar{\sigma}}) n_{3\bar{\sigma}} n_{4\sigma} - n_{2\bar{\sigma}} (1 - n_{3\bar{\sigma}}) \\ &\times (1 - n_{4\sigma}) + \delta_{14} [(1 - n_{1\sigma})(1 - n_{2\bar{\sigma}}) n_{3\bar{\sigma}} \\ &- n_{1\sigma} n_{2\bar{\sigma}} (1 - n_{3\bar{\sigma}}) (-1)] \} \delta_{\Delta\varepsilon,0} \delta_{1+2,3+4}. \end{aligned} \quad (39)$$

Here we kept the initial form of the equation and used the second half with  $\delta_{14}$  to show explicitly the additional term generated in the case of coinciding momenta  $\mathbf{1}$  and  $\mathbf{4}$ . As we see, Eq. (39) obeys the  $A/B/C/D$  form discussed in the previous section.

We can conclude that the rules presented till now allow us to calculate both collision integrals and linear response coefficients for the interactions with any number of secondary-quantization operators, using the FFT-accelerated approach. While the matrix elements were assumed

independent of momentum, we get rid of this restriction in the next section.

## VI. GENERALIZATION TO MOMENTUM-DEPENDENT MATRIX ELEMENTS

Now we generalize the approach to the case of nonconstant matrix element.

Let us consider the pair interaction in the form

$$\hat{H}_{\text{int}} = \sum_{\mathbf{k}\mathbf{p}\mathbf{q}} U_{\mathbf{q}} \hat{a}_{\mathbf{k}}^{\dagger} \hat{a}_{\mathbf{p}}^{\dagger} \hat{a}_{\mathbf{p}+\mathbf{q}} \hat{a}_{\mathbf{k}-\mathbf{q}}. \quad (40)$$

The components  $w_1^{(v)}$  in Eq. (22) are written as

$$w_1^{(v)} = \sum_{234} |U_{2-3}|^2 B_2^{(v)} C_3^{(v)} D_4^{(v)} \delta_{1+2,3+4} f(\Delta\varepsilon), \quad (41)$$

and after conversion to variables  $(\mathbf{r}, \gamma)$  become

$$W_{\mathbf{r}\gamma}^{(v)} = \left[ \sum_{\mathbf{r}'} u_{\mathbf{r}'} B_{-\mathbf{r}-\mathbf{r}',-\gamma}^{(v)} C_{\mathbf{r}+\mathbf{r}',\gamma}^{(v)} \right] D_{\mathbf{r},\gamma}^{(v)} F(\gamma), \quad (42)$$

with

$$w_{\mathbf{k}}^{(v)} = \mathcal{F}_{\mathbf{k},\varepsilon_{\mathbf{k}}}^{-1} \{W_{\mathbf{r}\gamma}^{(v)}\},$$

where  $u_{\mathbf{r}'}$  denotes the Fourier transform of  $(U_{\mathbf{q}})^2$ .

As we see, the expression inside square brackets is the discrete convolution of the array  $u_{\mathbf{r}}$  and the combination

$$M_{\mathbf{r}\gamma}^{(v)} \equiv B_{\mathbf{r},-\gamma}^{(v)} C_{-\mathbf{r},\gamma}^{(v)}$$

in 3D  $\mathbf{r}$  space and therefore can be calculated using an additional Fourier transform:

$$\begin{aligned} W_{\mathbf{r}\gamma}^{(v)} &= (u * M_{\gamma}^{(v)})_{-\mathbf{r}} D_{\mathbf{r},\gamma}^{(v)} F(\gamma) \\ &= \{ \mathcal{F}_{\mathbf{q} \rightarrow \mathbf{r}} [ (U_{\mathbf{q}})^2 \cdot M_{\mathbf{q}\gamma}^{(v)} ] \}_{-\mathbf{r}} D_{\mathbf{r},\gamma}^{(v)} F(\gamma). \end{aligned}$$

The other terms containing Kronecker delta for coinciding momenta, unfortunately, do not have the same convolution structure and cannot be calculated with the Fourier approach discussed till now. Still, we can use the fact that the number of summation terms here is lower than in the first case. For instance, consider the terms with  $\delta_{12}$ :

$$y_{\mathbf{k}}^{(v)} = \sum_{\mathbf{q}} |U_{\mathbf{q}}|^2 C_{\mathbf{k}+\mathbf{q}}^{(v)} D_{\mathbf{k}-\mathbf{q}}^{(v)} f(2\varepsilon_{\mathbf{k}} - \varepsilon_{\mathbf{k}+\mathbf{q}} - \varepsilon_{\mathbf{k}-\mathbf{q}}). \quad (43)$$

While the full number of calculations in (43) can be estimated as  $\{\mathbf{k} \times \mathbf{q}\} \sim L^6$ , the restriction for energy  $2\varepsilon_{\mathbf{k}} \simeq \varepsilon_{\mathbf{k}+\mathbf{q}} + \varepsilon_{\mathbf{k}-\mathbf{q}}$  limits the number of matching terms in each sum to  $N_{\mathbf{k}}^{(\text{terms})} \leq N_{\text{max}}^{(\text{terms})} \ll L^3$ . The relevant terms can be counted and tabulated in advance, making the number of calculations not exceed  $N_{\text{max}}^{(\text{terms})} L^3 \ll L^6$ .

The rest of the Kronecker-limited terms are handled with the same reasoning. As a result, the ultimate calculation complexity does not exceed  $\sim L^5 \ln L$ , which allows us to build the universal calculation-efficient scheme.

## VII. COMPUTER LIBRARY

To verify the correctness of the transformation, the results of the calculation using the accelerated relations were

compared with the direct summation of the original expressions for several small systems with  $L = 4, 6, 8$ , with various interaction types and particle statistics. The resulting numbers were equal with the precision of  $10 \div 13$  digits for each problem parameters, proving the validity of the presented approach and completeness of the rule set.

The calculation scheme described in this paper was realized in the form of computer Fortran 90 library FLBE (Fast Library for Boltzmann Equation) [29], applicable to a wide spectrum of condensed matter physics problems. It allows to obtain both collision integrals and linear response coefficients, and perform numerical simulation of kinetics with universal estimation of calculation complexity  $\sim L^5 \ln L$ , regardless of the interaction type.

The system under consideration can consist of several subsystems with Fermi and Bose statistics—electrons, phonons, excitons, photons, etc.—with various energy spectrum  $\varepsilon_{\mathbf{k}}$ , and arbitrary interaction terms. The corresponding single-particle Hamiltonian is

$$\hat{H}_0 = \sum_{\alpha,\mathbf{k}} \varepsilon_{\alpha,\mathbf{k}} \hat{n}_{\alpha,\mathbf{k}},$$

where  $\alpha$  denotes the sort of particles, i.e., subsystem.

The interaction terms

$$\hat{H}_{\text{int}} = \sum_j \hat{V}^{(j)} \quad (44)$$

are written in the form of ordered chain of secondary-quantization operators,

$$\hat{V}^{(j)} = \sum_{\{\mathbf{k}\},\{\mathbf{p}\}} U^{(j)}(\dots) \hat{a}_{\mathbf{k}_1}^{\dagger} \hat{b}_{\mathbf{k}_2}^{\dagger} \dots \hat{c}_{\mathbf{p}_2} \hat{d}_{\mathbf{p}_1},$$

such as pair interaction (5), (40), or electron-phonon interaction (29). Generally, any combination of operators is supported, with two restrictions: (i) we assume the momentum conservation

$$\sum \mathbf{k}_i = \sum \mathbf{p}_i,$$

and (ii) the matrix element can either be constant, like  $U_0$  in (5), or depend only on the momentum change, like  $U_{\mathbf{q}}$  in (40). More complicated interaction types with matrix elements depending on several momenta, e.g.,  $U(\mathbf{k}_1, \mathbf{k}_2, \dots)$ , are not supported currently due to limitations of the analytic transformation described in this paper.

The problem parameters are assumed dimensionless and the scale of time is determined by  $2\pi/\hbar = 1$ .

The primitive approach with direct summation of terms with calculation complexity  $\sim L^9$  is also realized in the library, as well as the wide set of automatic tests, allowing us to check the results of different approaches in case of doubt. Such variety can be especially useful in the case of nonstandard model.

The library performance and memory consumption is shown in Figs. 1–3. The data was obtained on Intel i9-10980XE 18-core CPU, 64 GB RAM, OS Linux (kernel version 5.4.0-91), and gcc Fortran compiler (version 9.3.0). We simulated the particle kinetics in lattice Bose gas with Hubbard interaction described by Eqs. (1), (2), and (4).

The memory consumption is determined by the auxiliary arrays in 4D  $[\mathbf{k}, \varepsilon]$  space required for Fourier transforms

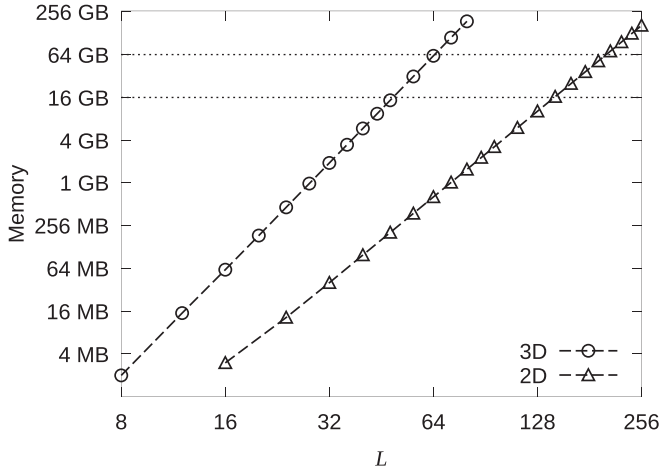


FIG. 1. Memory consumption for the problem (1), depending on the lattice size. Dotted horizontal lines mark popular RAM sizes 16 GB and 64 GB for easy estimation.

used in the accelerated approach. Due to real-valued input data  $\{n_{\alpha,\mathbf{k}}\}$ , the algorithm makes use of real-to-complex and complex-to-real versions of FFT so the auxiliary arrays consist of 8-byte double precision real values.

The dimensions of each array are  $L^d \times 2N_\varepsilon$ , where  $N_\varepsilon$  is determined by the maximal energy value in the particle spectrum. For the Bose system with the parabolic dispersion law used in the benchmark, the spectrum is equidistant  $\varepsilon_{\mathbf{k}} = \varepsilon_1 \mathbf{k}^2$ , and the maximal value of energy is reached at the momentum  $\mathbf{k}$  at the edge of Brillouin zone with indexes  $k_\alpha = -L/2$ , therefore  $N_\varepsilon$  equals to  $3L^2/4$  or  $L^2/2$  for 3D or 2D, correspondingly. As a result, the array volume is

$$V_a^{(3D)} = 12L^5, \tag{45}$$

$$V_a^{(2D)} = 8L^4. \tag{46}$$

For the case of  $N_S$  subsystems in the problem,  $2N_S + 5$  arrays are needed.

As we see in Fig. 1, the systems with size more than  $L = 128$  for 2D and up to  $L = 64$  for 3D can be simulated with 64 GB RAM. Still, it could be recommended to use a smaller size to save the computing resources:  $L = 64 \div 80$  for 2D and  $L = 28 \div 36$  for 3D are large enough to approach the macroscopic behavior and still take no more than a few seconds per calculation step (see Fig. 2). We see that the FFT-accelerated approach v4 obeys approximately the expected  $\sim L^{d+2} \ln L$  scaling. The versions employing direct summation of terms v1 and v0 demonstrate much higher times  $\sim L^{d.3} = V^3$ .

For the problems with nonequidistant spectrum, the appropriate energy discretization step  $\Delta\varepsilon_{\text{calc}}$  should be used, as discussed in Sec. III, increasing the memory consumption and amount of calculations. This fact should be taken into account when planning the research and choosing the system size.

The library benefits from multithreading, as the calculation is based on FFT, which allows complete parallelization. In Fig. 3, we show the performance for different number of OpenMP threads. The efficiency gain for eight threads is

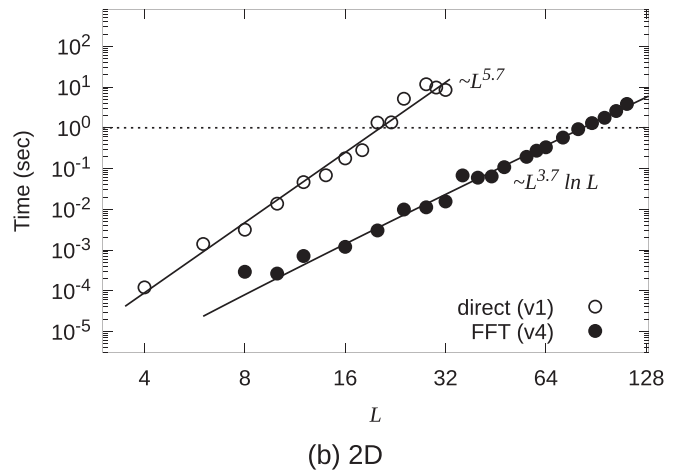
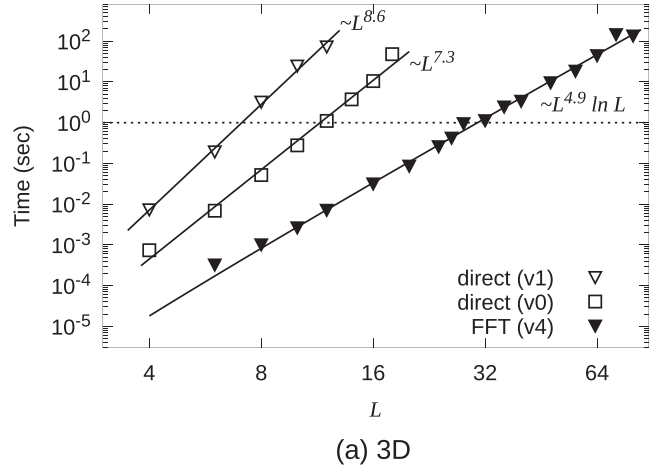


FIG. 2. Time per step: Time to calculate the array of collision integrals  $J_{\mathbf{k}}$  depending on lattice size: (a) 3D and (b) 2D. Values for several algorithm versions are presented: v4 is the accelerated approach described in this paper, v1 employs direct summation of terms, and v0 is the special highly optimized version of the direct summation approach written explicitly for the 3D problem with pair interaction term (5) of Sec. II. Solid lines show the theoretical fitting indicated near to the line. Dotted horizontal line marks the one-second cutoff to indicate the practically affordable system sizes.

usually  $5x \dots 7x$ , depending on the specific system size under study.

The directions of the library development include the creation of interfaces for other programming languages, expansion to MPI technology for use on computing clusters, and incorporation of GPGPU calculations (CUDA or OpenCL), as well as application to the wider set of physical problems demanded by experiment.

### VIII. EXAMPLE OF APPLICATION

Finally, to demonstrate the efficiency and reliability of the approach, we simulate the relaxation of the excited state in several relevant problems of condensed matter physics.

*a. Electron gas in metal after absorption of ultrashort laser pulse.* This problem is related to pump-probe scanning experiments and laser processing of metals using femtosecond

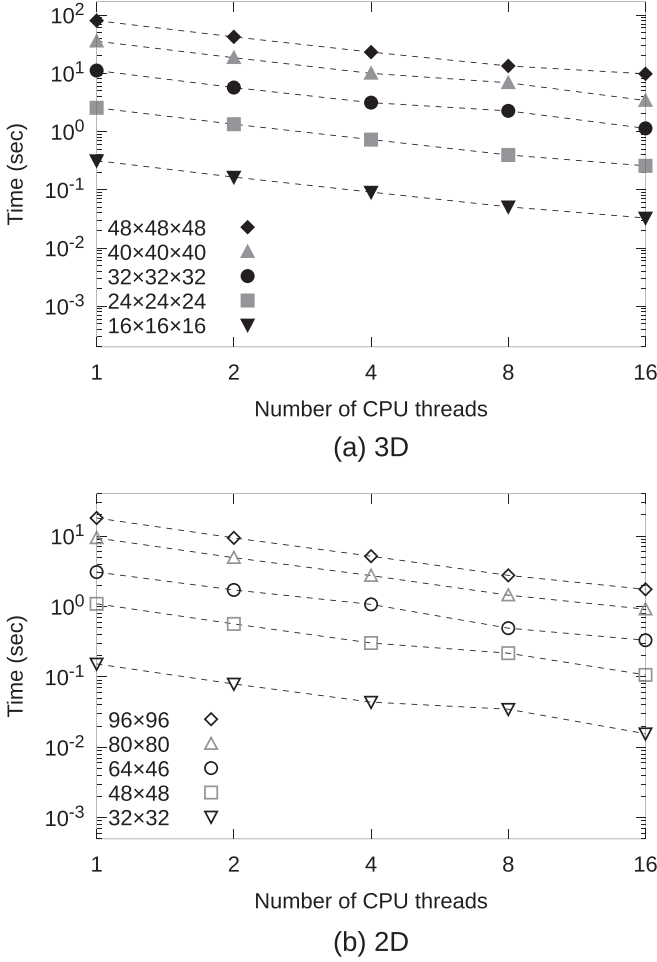


FIG. 3. Time per step, depending on the number of CPU threads: (a) 3D and (b) 2D. Dashed lines are to guide the eye.

pulses. In Fig. 4, we show the result of kinetics simulation in a qualitative model of conduction electrons in metal after excitation, demonstrating typical relaxation to thermal distribution function [38].

The initial excitation was taken in the form [19]

$$\delta n_{\mathbf{k}}(t=0) \sim \xi_{\mathbf{k}} \exp[-(\xi_{\mathbf{k}}/\sigma)^2],$$

where  $\xi_{\mathbf{k}} \equiv \varepsilon_{\mathbf{k}} - E_F$ ,  $\varepsilon_{\mathbf{k}} = \varepsilon_1 k^2$  is the electron dispersion law,  $E_F$  is the Fermi energy, and  $\sigma$  is the spectral width of the source.

Due to high concentration of the current carriers in metal, the electron-electron pair interaction is described by the screened Coulomb interaction:

$$U_{\mathbf{q}}^{(c)} = \frac{U^{(c)}}{\mathbf{q}^2 + k_0^2}, \quad (47)$$

where  $k_0 \equiv 1/\lambda_D$  and  $\lambda_D$  is the Debye screening length. As the matrix elements (47) depend on the momentum change  $\mathbf{q}$ , the calculation of collision integrals was performed using the formulas given in Sec. VI. The phonon subsystem was excluded from the model due to very short times of electron processes in metals [5,6], defining the main characteristics of the relaxation process in the case under consideration.

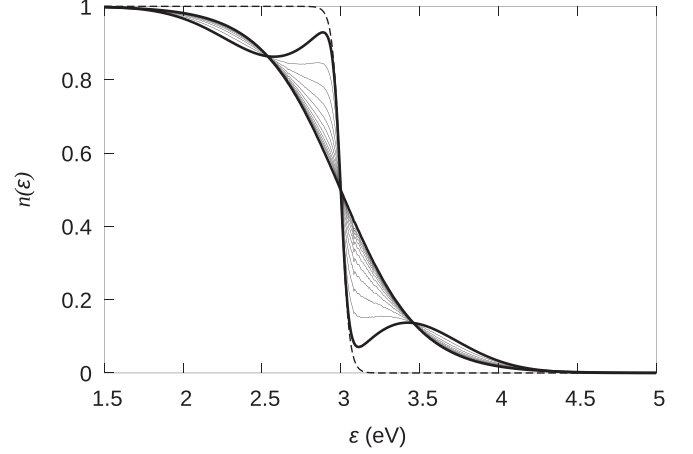


FIG. 4. Result of simulation: Relaxation of electron distribution function in metal after excitation. Model parameters: Debye screening wave number  $k_0 = (1/8)\pi/a$ , Fermi wave number  $k_F = (3/4)\pi/a$ , Fermi energy  $E_F = 3.0$  eV, initial temperature  $T = 0.026$  eV, spectral width of the source  $\sigma = 0.6$  eV. The distribution functions are presented at time points with step  $\Delta t_1 = 4 \times 10^{-3}$  A.u. Initial state before the excitation is shown with dashed line, the distribution right after the pulse absorption and the final equilibrium distribution are emphasized with bold. Momentum grid dimensions:  $64 \times 64 \times 64$ , total size of work arrays 61.5 GB, time of calculation 107 s per step.

The parabolic dispersion law of electrons in the conduction band allowed us to employ the approach version for equidistant energy levels described in Sec. II, resulting in exact energy conservation. During the whole calculation, the particle number and total energy in the system remained constant with precision of 14 and 11 digits, correspondingly. This shows the stability of the method, allowing us to study various problems of a similar type.

*b. Sympathetic cooling in the mixture of two species of particles.* It is used in the experiments on laser cooling and Bose-Einstein condensation of atomic gases. Here, the initial state of both subsystems is thermal but with different temperatures. Particle collisions result in the energy exchange between the hotter and colder subsystems and gradual temperature equalization. This technique is especially useful for efficient cooling of Fermi atoms. There are known experiments with Fermi-Bose mixtures [39], Fermi-Fermi [40], Bose-Bose [41–44], and three-species Fermi-Fermi-Bose [45], as well as the version with the same species in different atomic states [46].

In Fig. 5, we show the result of simulations for the mixture of two Bose gases (spin  $S = 0$ ) with initially different temperatures. The subsystem temperatures  $T_1, T_2$  show the behavior similar to experiments [43,44].

The temperatures were determined using the auxiliary function which has a linear form in the thermodynamic equilibrium state  $\ln[1/n_i(\varepsilon) + 1] \simeq (\varepsilon - \mu_i)/T_i$ , where  $\mu_i$  is the chemical potential of the corresponding system.

Pair interaction inside each subsystem and between the subsystems was taken momentum independent in the form (5) with equal amplitudes:

$$U_0^{(1-1)} = U_0^{(2-2)} = U_0^{(1-2)} = 1.$$

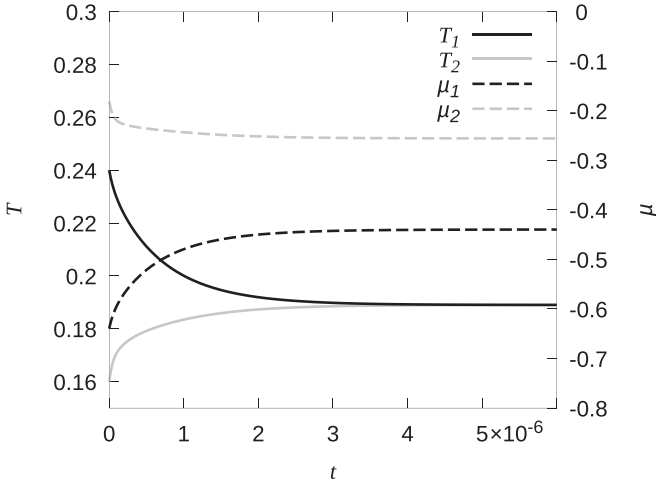


FIG. 5. Thermalization in the mixture of two species of Bose atoms with different initial temperatures. Dimensionless problem parameters: Atom masses  $M_1 = 87$ ,  $M_2 = 133$  (model  $^{87}\text{Rb}$  and  $^{133}\text{Cs}$  atoms), start temperatures  $T_1 = 0.24$ ,  $T_2 = 0.16$ , particle numbers  $N_1 = 300$ ,  $N_2 = 200$ . Momentum grid dimensions:  $32 \times 32 \times 32$ , the level broadening width used in the calculation  $\Gamma = 10^{-3}$ , resulting in total size of work arrays 15.5 GB and calculation time 42 s per step.

Inequal atom masses result in the more complicated energy spectrum of the system under study. As we discussed in Sec. III, to study the system with nonequidistant levels, the finite level width should be introduced. This affects the total energy conservation. The smaller the level width, the smaller should be the energy discretization step, resulting in lower calculation performance and higher RAM requirements due to the increased size of work arrays. In Fig. 6, we show the precision of total energy conservation during the simulation with several values of level broadening width. We see that in

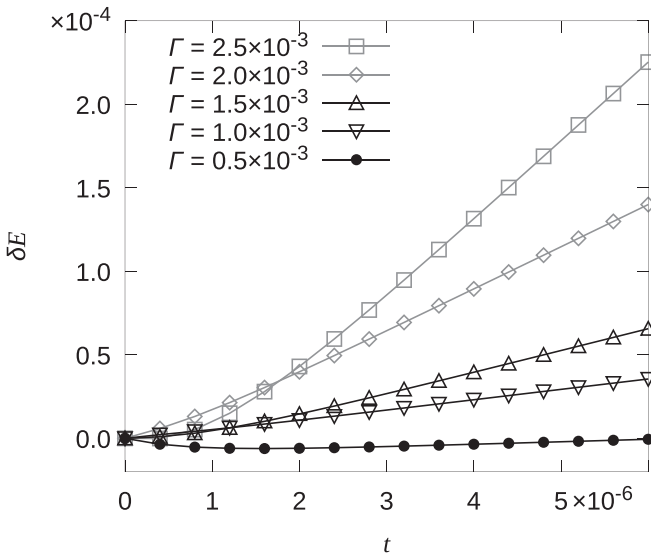


FIG. 6. Relative total energy change  $\delta E = \frac{E - E(t=0)}{E(t=0)}$  during the calculation for several values of level broadening  $\Gamma$  (Gaussian line shape). Energy discretization step equals broadening width  $\Delta \varepsilon_{\text{calc}} = \Gamma$ . Particle number remained virtually constant with the precision of 12 and more digits.

this case, the sufficient precision is achieved with  $\Gamma \leq 10^{-3}$ . As a conclusion, the choice of the level broadening to use in the simulation depends on the required precision and available computation resources.

*c. Relaxation of carriers in semiconductor after the injection of excess electrons with nonzero momentum.* Contrary to optical excitation, here the particle distribution is essentially asymmetric. A correct description of this problem is impossible without paying attention to the details of particle distribution in momentum space. The dispersion law of electrons and holes was taken following the tight-binding model [47]

$$\varepsilon_{\mathbf{k}}^{(e)} = \frac{\Delta}{2} - [\cos(k_x a) + \cos(k_y a) - 2], \quad (48)$$

$$\varepsilon_{\mathbf{k}}^{(h)} = -\varepsilon_{\mathbf{k}}^{(e)}, \quad (49)$$

where  $\Delta$  is the energy gap, hopping amplitude equals 0.5,  $a$  is the lattice constant, and indexes  $e, h$  denote electrons in conduction band or holes in valence band, respectively. The geometry is considered two-dimensional.

Pair interaction inside each band and between the bands was again taken momentum independent in the form (5) with equal amplitudes:

$$U_0^{(e-e)} = U_0^{(h-h)} = U_0^{(e-h)} = 1.$$

The density of the injected excess electrons was taken in the form of Gaussian function centered at the momentum point  $\mathbf{k}_c = (0.6, 0.6)\pi/a$  with half width  $0.1\pi/a$  and maximal amplitude  $\delta n^{(\text{max})} = 0.2$ . The distribution of original particles was calculated using inverse temperature  $1/T = 6.0$  and Fermi level in the middle of the band gap  $E_F = 0$ .

The energy axis discretization step and level broadening were taken as the fraction of the first excitation energy  $\Delta \varepsilon_{\text{calc}} = \Gamma = 0.2(1 - \cos \frac{2\pi}{L})$ , giving the total energy conservation precision as low as  $\delta E \sim 10^{-7}$ .

In Fig. 7, we show the calculated particle distributions at several time points after injection. Note the features of the momentum relaxation at the early stages. Two bright areas with noticeable occupation at axes  $k_x$  and  $k_y$  can be explained by the specific additive form of the dispersion law (48),

$$\varepsilon_{\mathbf{k}}^{(e)} = f_1(k_x) + f_1(k_y),$$

which enables efficient scattering of the injected electrons at momentum point  $(k_x, k_y)$  with the original particles around the point  $(0,0)$  to occupy the corresponding areas at axes  $k_x$  and  $k_y$  due to the conservation of energy:

$$\varepsilon_{(k_x, k_y)}^{(e)} + \varepsilon_{(0,0)}^{(e)} = \varepsilon_{(k_x, 0)}^{(e)} + \varepsilon_{(0, k_y)}^{(e)}.$$

The analogous bright areas in the valence band are explained similarly. In Fig. 8, we present the particle distribution along direction  $k_x = k_y$  to show the area of noticeable occupation at the momentum point  $-\mathbf{k}_c$  in the valence band, explained using Eq. (49).

In the case of different effective masses in the bands, or other form of dispersion law, the picture is expected to change accordingly. This gives an example of the physical problem benefiting from the detailed simulation of kinetics on fine momentum grid.



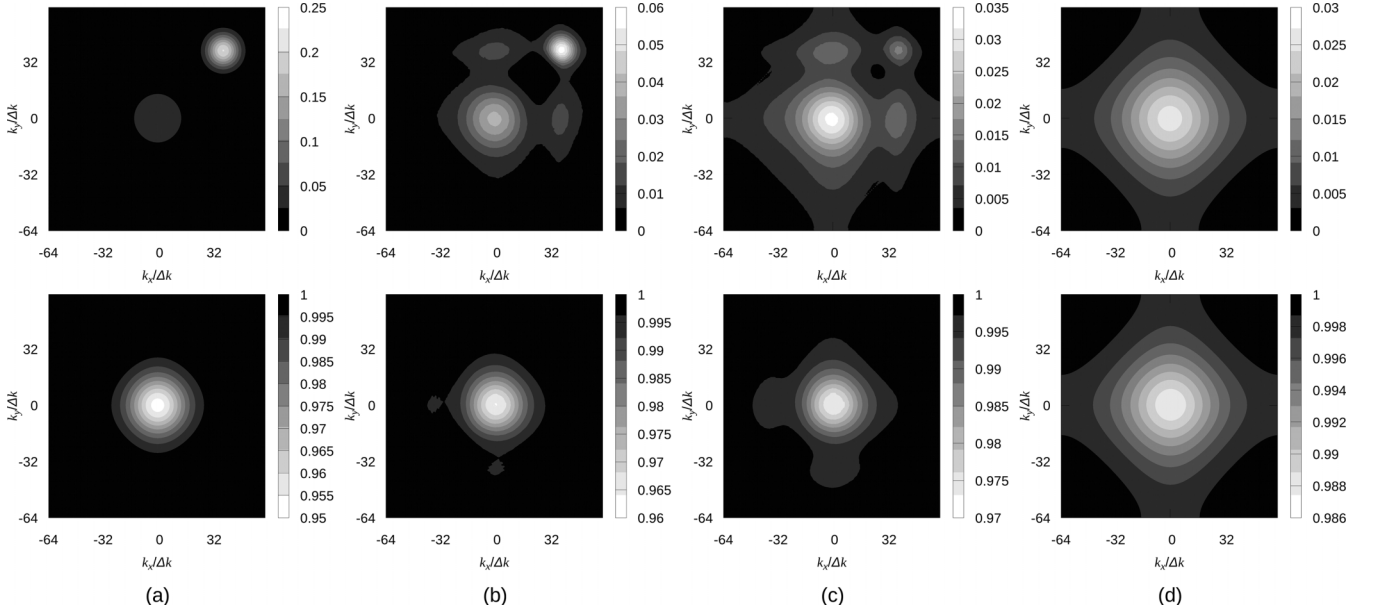


FIG. 7. Particle distributions (top: conduction band; bottom: valence band) in the first Brillouin zone at time points (a)  $t = 0$ , (b) 0.1, (c) 0.2, (d) 1.0 A.u. The problem parameters are given in main text. Dimension of 2D momentum grid used in calculation is  $L = 128$ , size of work arrays 29.1 GB, calculation time 97 s per step.

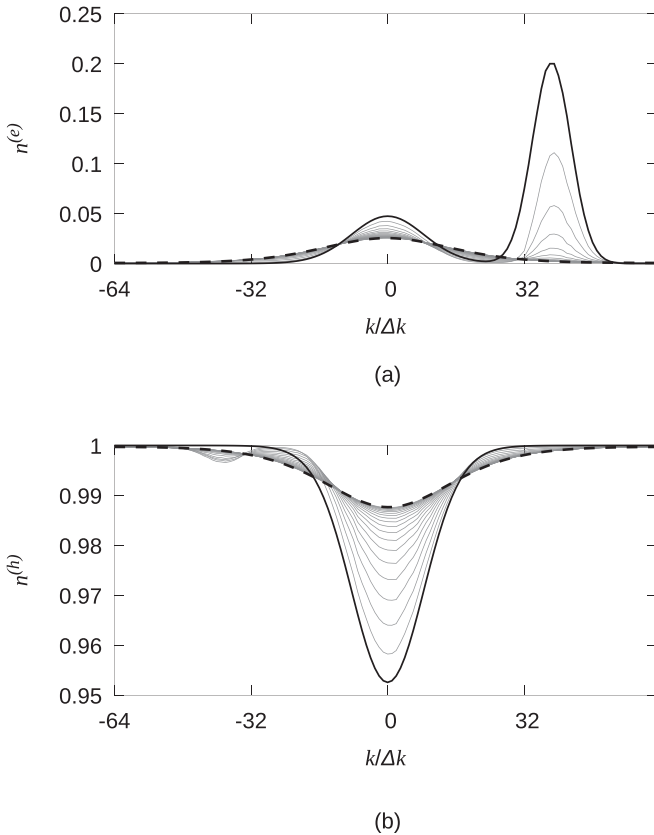


FIG. 8. Slices of distribution function  $n_{\mathbf{k}}^{(e,h)}$  at diagonal direction  $k_x = k_y$  during the relaxation, showing the temporary peak in hole occupation. The graphs are shown for time points with step  $\Delta t_1 = 0.05$  A.u. Bold and dashed lines show the initial and final distributions, respectively.

## IX. CONCLUSION

We describe a general method for efficient calculation of Boltzmann collision integrals on a discrete momentum lattice, useful for a wide spectrum of solid-state problems. The original analytical transformation allows us to work with an arbitrary single-particle spectrum as well as momentum-dependent interactions.

The universal set of transformation rules is presented in detail and realized in the form of computer Fortran 90 library [29]. Due to application of the FFT, the calculation complexity is lowered from  $\sim L^9$  to  $\sim L^5 \ln L$ . As a result, the affordable lattice size can be up to  $L = 64$  for 3D and more than  $L = 128$  for 2D on a desktop workstation, which allows us to study continual systems using appropriate extrapolation.

The precision and flexibility of the presented approach is demonstrated by simulation of nonequilibrium state relaxation in three problems of condensed matter physics. Overall, it can be applied to Bose and Fermi systems of various complexities. This enables efficient numerical study of kinetics in the problems of modern experiments, such as relaxation of ultracold atomic gases in magneto-optical traps [48], evolution of optically excited carriers in semiconductors [49] and metals [5], effects of ultrashort pulses, and transport current on superconductivity [50], etc.

## ACKNOWLEDGMENTS

This work was supported by the Ministry of Science and Higher Education of the Russian Federation (state task Project No. FSWU-2023-0031). The development of Secs. VI–VII was supported by MPhI Program Priority 2030.

## APPENDIX: TRANSFORMATION

In this Appendix, we show how to convert Eqs. (7) and (8) to (16)–(19).

We start from Eq. (8) for Bose statistics in the form (A1) expanding the brackets and grouping the terms with similar Kronecker delta:

$$J_{\mathbf{k}_1} = 2U_0^2 \sum_{\mathbf{k}_2 \mathbf{k}_3 \mathbf{k}_4} \{ [n_{\mathbf{k}_2} n_{\mathbf{k}_3} n_{\mathbf{k}_4} + n_{\mathbf{k}_3} n_{\mathbf{k}_4} + n_{\mathbf{k}_1} (n_{\mathbf{k}_3} n_{\mathbf{k}_4} - n_{\mathbf{k}_2} n_{\mathbf{k}_3} - n_{\mathbf{k}_2} n_{\mathbf{k}_4} - n_{\mathbf{k}_2})] - \delta_{34} [(n_{\mathbf{k}_2} n_{\mathbf{k}_3} + n_{\mathbf{k}_3}) + n_{\mathbf{k}_1} (2n_{\mathbf{k}_2} n_{\mathbf{k}_3} + n_{\mathbf{k}_2} + n_{\mathbf{k}_3})] + \delta_{12} [n_{\mathbf{k}_3} n_{\mathbf{k}_4} + n_{\mathbf{k}_1} (2n_{\mathbf{k}_3} n_{\mathbf{k}_4} + n_{\mathbf{k}_3} + n_{\mathbf{k}_4} + 1)] + \delta_{12} \delta_{34} (n_{\mathbf{k}_1} - n_{\mathbf{k}_3}) \} \delta_{\varepsilon_1 + \varepsilon_2, \varepsilon_3 + \varepsilon_4} \delta_{\mathbf{k}_1 + \mathbf{k}_2, \mathbf{k}_3 + \mathbf{k}_4}. \quad (\text{A1})$$

*a. The first square bracket.* It can be conveniently written as

$$J_{\mathbf{k}_1}^{(1)} = 2U_0^2 \{ w_{\mathbf{k}_1}^{(234)} + w_{\mathbf{k}_1}^{(34)} + n_{\mathbf{k}_1} [w_{\mathbf{k}_1}^{(34)} - 2w_{\mathbf{k}_1}^{(23)} - w_{\mathbf{k}_1}^{(2)}] \}, \quad (\text{A2})$$

where

$$w_{\mathbf{k}_1}^{(234)} \equiv \sum_{\mathbf{k}_2 \dots \mathbf{k}_4} n_{\mathbf{k}_2} n_{\mathbf{k}_3} n_{\mathbf{k}_4} \delta_{\varepsilon_1 + \varepsilon_2, \varepsilon_3 + \varepsilon_4} \delta_{\mathbf{k}_1 + \mathbf{k}_2, \mathbf{k}_3 + \mathbf{k}_4}, \quad (\text{A3})$$

$$w_{\mathbf{k}_1}^{(34)} \equiv \sum_{\mathbf{k}_2 \mathbf{k}_3 \mathbf{k}_4} n_{\mathbf{k}_3} n_{\mathbf{k}_4} \delta_{\varepsilon_1 + \varepsilon_2, \varepsilon_3 + \varepsilon_4} \delta_{\mathbf{k}_1 + \mathbf{k}_2, \mathbf{k}_3 + \mathbf{k}_4}, \quad (\text{A4})$$

$$w_{\mathbf{k}_1}^{(23)} \equiv \sum_{\mathbf{k}_2 \mathbf{k}_3 \mathbf{k}_4} n_{\mathbf{k}_2} n_{\mathbf{k}_3} \delta_{\varepsilon_1 + \varepsilon_2, \varepsilon_3 + \varepsilon_4} \delta_{\mathbf{k}_1 + \mathbf{k}_2, \mathbf{k}_3 + \mathbf{k}_4}, \quad (\text{A5})$$

$$w_{\mathbf{k}_1}^{(2)} \equiv \sum_{\mathbf{k}_2 \mathbf{k}_3 \mathbf{k}_4} n_{\mathbf{k}_2} \delta_{\varepsilon_1 + \varepsilon_2, \varepsilon_3 + \varepsilon_4} \delta_{\mathbf{k}_1 + \mathbf{k}_2, \mathbf{k}_3 + \mathbf{k}_4}. \quad (\text{A6})$$

Let us rewrite expression (A3) in the expanded space  $(\mathbf{k}, \varepsilon) \equiv \kappa$ , employ the notation from Eqs. (12)–(15), and replace Kronecker delta with sums

$$w_{\mathbf{k}_1 \varepsilon_1}^{(234)} = \frac{1}{L^3 N_\varepsilon} \sum_{\substack{\mathbf{k}_2 \mathbf{k}_3 \mathbf{k}_4 \\ \varepsilon_2 \varepsilon_3 \varepsilon_4}} n_{\mathbf{k}_2 \varepsilon_2} n_{\mathbf{k}_3 \varepsilon_3} n_{\mathbf{k}_4 \varepsilon_4} \times \sum_{\mathbf{r}\gamma} e^{i(\mathbf{k}_1 + \mathbf{k}_2 - \mathbf{k}_3 - \mathbf{k}_4)\mathbf{r}} e^{i(\varepsilon_1 + \varepsilon_2 - \varepsilon_3 - \varepsilon_4)\gamma}. \quad (\text{A7})$$

Using the relation  $n_{\mathbf{k}\varepsilon} = \sum_{\mathbf{r}\gamma} N_{\mathbf{r}\gamma} e^{i(\mathbf{k}\mathbf{r} + \varepsilon\gamma)}$ , we can write

$$w_{\mathbf{k}_1 \varepsilon_1}^{(234)} = \frac{1}{L^3 N_\varepsilon} \sum_{\substack{\mathbf{k}_2 \mathbf{k}_3 \mathbf{k}_4 \\ \varepsilon_2 \varepsilon_3 \varepsilon_4}} \sum_{\substack{\mathbf{r}_2 \mathbf{r}_3 \mathbf{r}_4 \\ \gamma_2 \gamma_3 \gamma_4}} N_{\mathbf{r}_2 \gamma_2} N_{\mathbf{r}_3 \gamma_3} N_{\mathbf{r}_4 \gamma_4} \times \sum_{\mathbf{r}\gamma} e^{i(\mathbf{k}_2 \mathbf{r}_2 + \mathbf{k}_3 \mathbf{r}_3 + \mathbf{k}_4 \mathbf{r}_4)} e^{i(\varepsilon_2 \gamma_2 + \varepsilon_3 \gamma_3 + \varepsilon_4 \gamma_4)} \times e^{i(\mathbf{k}_1 + \mathbf{k}_2 - \mathbf{k}_3 - \mathbf{k}_4)\mathbf{r}} e^{i(\varepsilon_1 + \varepsilon_2 - \varepsilon_3 - \varepsilon_4)\gamma} = \frac{1}{L^3 N_\varepsilon} \sum_{\mathbf{r}\gamma} N_{-\mathbf{r}, -\gamma} N_{\mathbf{r}\gamma} N_{\mathbf{r}\gamma} e^{i(\mathbf{k}_1 \mathbf{r} + \varepsilon_1 \gamma)}, \quad (\text{A8})$$

which has the form of the inverse Fourier transform. After that, the desired values  $w_{\mathbf{k}}^{(234)}$  for the expression (A2) can be obtained by putting the second index  $\varepsilon = \varepsilon_{\mathbf{k}}$ :

$$w_{\mathbf{k}}^{(234)} = \mathcal{F}_{\mathbf{k}\varepsilon_{\mathbf{k}}}^{-1} \{ N_{-\mathbf{r}, -\gamma} (N_{\mathbf{r}\gamma})^2 \}. \quad (\text{A9})$$

The expressions for  $w^{(34)}$ ,  $w^{(23)}$ ,  $w^{(2)}$  can be converted in the same way. As a result, we obtain

$$w_{\mathbf{k}}^{(34)} = \mathcal{F}_{\mathbf{k}\varepsilon_{\mathbf{k}}}^{-1} \{ S_{-\mathbf{r}, -\gamma} (N_{\mathbf{r}\gamma})^2 \}, \quad (\text{A10})$$

$$w_{\mathbf{k}}^{(23)} = \mathcal{F}_{\mathbf{k}\varepsilon_{\mathbf{k}}}^{-1} \{ N_{-\mathbf{r}, -\gamma} N_{\mathbf{r}\gamma} S_{\mathbf{r}\gamma} \}, \quad (\text{A11})$$

$$w_{\mathbf{k}}^{(2)} = \mathcal{F}_{\mathbf{k}\varepsilon_{\mathbf{k}}}^{-1} \{ N_{-\mathbf{r}, -\gamma} (S_{\mathbf{r}\gamma})^2 \}, \quad (\text{A12})$$

where  $S_{\mathbf{r}\gamma}$  is the Fourier transform of the function  $s_{\mathbf{k}\varepsilon} \equiv \delta_{\varepsilon, \varepsilon_{\mathbf{k}}}$ .

*b. The second square bracket.* It corresponds to the case when  $\mathbf{k}_3 = \mathbf{k}_4$ . It can be written as

$$J_{\mathbf{k}_1}^{(2)} = -2U_0^2 \{ [x_{\mathbf{k}_1}^{(23)} + x_{\mathbf{k}_1}^{(3)}] + n_{\mathbf{k}_1} [2x_{\mathbf{k}_1}^{(23)} + x_{\mathbf{k}_1}^{(3)} + x_{\mathbf{k}_1}^{(2)}] \}, \quad (\text{A13})$$

where

$$x_{\mathbf{k}_1}^{(23)} \equiv \sum_{\mathbf{k}_2 \mathbf{k}_3 \mathbf{k}_4} n_{\mathbf{k}_2} n_{\mathbf{k}_3} \delta_{\mathbf{k}_3, \mathbf{k}_4} \delta_{\varepsilon_1 + \varepsilon_2, \varepsilon_3 + \varepsilon_4} \delta_{\mathbf{k}_1 + \mathbf{k}_2, \mathbf{k}_3 + \mathbf{k}_4}, \quad (\text{A14})$$

$$x_{\mathbf{k}_1}^{(3)} \equiv \sum_{\mathbf{k}_2 \mathbf{k}_3 \mathbf{k}_4} n_{\mathbf{k}_3} \delta_{\mathbf{k}_3, \mathbf{k}_4} \delta_{\varepsilon_1 + \varepsilon_2, \varepsilon_3 + \varepsilon_4} \delta_{\mathbf{k}_1 + \mathbf{k}_2, \mathbf{k}_3 + \mathbf{k}_4}, \quad (\text{A15})$$

$$x_{\mathbf{k}_1}^{(2)} \equiv \sum_{\mathbf{k}_2 \mathbf{k}_3 \mathbf{k}_4} n_{\mathbf{k}_2} \delta_{\mathbf{k}_3, \mathbf{k}_4} \delta_{\varepsilon_1 + \varepsilon_2, \varepsilon_3 + \varepsilon_4} \delta_{\mathbf{k}_1 + \mathbf{k}_2, \mathbf{k}_3 + \mathbf{k}_4}. \quad (\text{A16})$$

The reasoning similar to the previous paragraph gives the expressions

$$x_{\mathbf{k}}^{(23)} = \mathcal{F}_{\mathbf{k}\varepsilon_{\mathbf{k}}}^{-1} \{ N_{-\mathbf{r}, -\gamma} N_{2\mathbf{r}2\gamma} \}, \quad (\text{A17})$$

$$x_{\mathbf{k}}^{(3)} = \mathcal{F}_{\mathbf{k}\varepsilon_{\mathbf{k}}}^{-1} \{ S_{-\mathbf{r}, -\gamma} N_{2\mathbf{r}2\gamma} \}, \quad (\text{A18})$$

$$x_{\mathbf{k}}^{(2)} = \mathcal{F}_{\mathbf{k}\varepsilon_{\mathbf{k}}}^{-1} \{ N_{-\mathbf{r}, -\gamma} S_{2\mathbf{r}2\gamma} \}. \quad (\text{A19})$$

*c. The third square bracket.* It corresponds to the case when  $\mathbf{k}_1 = \mathbf{k}_2$ . Taking into consideration the same role of  $\mathbf{k}_3$  and  $\mathbf{k}_4$  in the sums, we can write

$$J_{\mathbf{k}_1}^{(3)} = 2U_0^2 \{ y_{\mathbf{k}_1}^{(34)} + n_{\mathbf{k}_1} [2y_{\mathbf{k}_1}^{(34)} + 2y_{\mathbf{k}_1}^{(3)} + y_{\mathbf{k}_1}^{(0)}] \}, \quad (\text{A20})$$

where

$$y_{\mathbf{k}_1}^{(34)} \equiv \sum_{\mathbf{k}_2 \mathbf{k}_3 \mathbf{k}_4} n_{\mathbf{k}_3} n_{\mathbf{k}_4} \delta_{\mathbf{k}_1, \mathbf{k}_2} \delta_{\varepsilon_1 + \varepsilon_2, \varepsilon_3 + \varepsilon_4} \delta_{\mathbf{k}_1 + \mathbf{k}_2, \mathbf{k}_3 + \mathbf{k}_4}, \quad (\text{A21})$$

$$y_{\mathbf{k}_1}^{(3)} \equiv \sum_{\mathbf{k}_2 \mathbf{k}_3 \mathbf{k}_4} n_{\mathbf{k}_3} \delta_{\mathbf{k}_1, \mathbf{k}_2} \delta_{\varepsilon_1 + \varepsilon_2, \varepsilon_3 + \varepsilon_4} \delta_{\mathbf{k}_1 + \mathbf{k}_2, \mathbf{k}_3 + \mathbf{k}_4}, \quad (\text{A22})$$

$$y_{\mathbf{k}_1}^{(0)} \equiv \sum_{\mathbf{k}_2 \mathbf{k}_3 \mathbf{k}_4} \delta_{\mathbf{k}_1, \mathbf{k}_2} \delta_{\varepsilon_1 + \varepsilon_2, \varepsilon_3 + \varepsilon_4} \delta_{\mathbf{k}_1 + \mathbf{k}_2, \mathbf{k}_3 + \mathbf{k}_4}. \quad (\text{A23})$$

Repeating the transformation made in (A7), we convert Eq. (A21) to the form

$$y_{\mathbf{k}_1 \varepsilon_1}^{(34)} = \frac{1}{L^3 N_\varepsilon} \sum_{\mathbf{r}_\gamma} N_{\mathbf{r}_\gamma} N_{\mathbf{r}_\gamma} e^{i(2\mathbf{k}_1 \mathbf{r} + 2\varepsilon_1 \gamma)}, \quad (\text{A24})$$

i.e., the required values of  $y_{\mathbf{k}_1 \varepsilon_1}^{(34)}$  are calculated using inverse Fourier transform with doubled indexes

$$y_{\mathbf{k}}^{(34)} = \mathcal{F}_{2\mathbf{k}, 2\varepsilon_k}^{-1} \{(N_{\mathbf{r}_\gamma})^2\}. \quad (\text{A25})$$

The expressions for the remaining values are obtained similarly:

$$y_{\mathbf{k}}^{(3)} = \mathcal{F}_{2\mathbf{k}, 2\varepsilon_k}^{-1} \{N_{\mathbf{r}_\gamma} S_{\mathbf{r}_\gamma}\}, \quad (\text{A26})$$

$$y_{\mathbf{k}}^{(0)} = \mathcal{F}_{2\mathbf{k}, 2\varepsilon_k}^{-1} \{(S_{\mathbf{r}_\gamma})^2\}. \quad (\text{A27})$$

*d. The last term.* It corresponds to the case when  $\mathbf{k}_1 = \mathbf{k}_2$  and  $\mathbf{k}_3 = \mathbf{k}_4$ . It can be written as

$$J_{\mathbf{k}_1}^{(4)} = 2U_0^2 [-z_{\mathbf{k}_1}^{(3)} + n_{\mathbf{k}_1} z_{\mathbf{k}_1}^{(0)}], \quad (\text{A28})$$

where

$$z_{\mathbf{k}_1}^{(3)} \equiv \sum_{\mathbf{k}_2 \mathbf{k}_3 \mathbf{k}_4} n_{\mathbf{k}_3} \delta_{\mathbf{k}_1, \mathbf{k}_2} \delta_{\mathbf{k}_3, \mathbf{k}_4} \delta_{\varepsilon_1 + \varepsilon_2, \varepsilon_3 + \varepsilon_4} \delta_{\mathbf{k}_1 + \mathbf{k}_2, \mathbf{k}_3 + \mathbf{k}_4}, \quad (\text{A29})$$

$$z_{\mathbf{k}_1}^{(0)} \equiv \sum_{\mathbf{k}_2 \mathbf{k}_3 \mathbf{k}_4} \delta_{\mathbf{k}_1, \mathbf{k}_2} \delta_{\mathbf{k}_3, \mathbf{k}_4} \delta_{\varepsilon_1 + \varepsilon_2, \varepsilon_3 + \varepsilon_4} \delta_{\mathbf{k}_1 + \mathbf{k}_2, \mathbf{k}_3 + \mathbf{k}_4}. \quad (\text{A30})$$

Repeating the conversions made for the second and third lines, we obtain the relations

$$z_{\mathbf{k}}^{(3)} = \mathcal{F}_{2\mathbf{k}, 2\varepsilon_k}^{-1} (N_{2\mathbf{r}, 2\gamma}), \quad (\text{A31})$$

$$z_{\mathbf{k}}^{(0)} = \mathcal{F}_{2\mathbf{k}, 2\varepsilon_k}^{-1} (S_{2\mathbf{r}, 2\gamma}). \quad (\text{A32})$$

Combining all the terms, we get the expressions (18) and (19). The relations for Fermi statistics are derived using the same reasoning.

- 
- [1] M. Chini, K. Zhao, Z. Chang, The generation, characterization and applications of broadband isolated attosecond pulses, *Nature Photon* **8**, 178 (2014).
- [2] X. Wang, L. Wang, F. Xiao, D. Zhang, Z. Lü, J. Yuan, Z. Zhao, Generation of 88 as isolated attosecond pulses with double optical gating, *Chin. Phys. Lett.* **37**, 023201 (2020).
- [3] P. Kusar, V. V. Kabanov, J. Demsar, T. Mertelj, S. Sugai, and D. Mihailovic, Controlled Vaporization of the Superconducting Condensate in Cuprate Superconductors by Femtosecond Photoexcitation, *Phys. Rev. Lett.* **101**, 227001 (2008).
- [4] A. S. Kurdyubov, A. V. Trifonov, I. Ya. Gerlovin, B. F. Gribakin, P. S. Grigoryev, A. V. Mikhailov, I. V. Ignatiev, Yu. P. Efimov, S. A. Eliseev, V. A. Lovtcius *et al.*, Optical control of a dark exciton reservoir, *Phys. Rev. B* **104**, 035414 (2021).
- [5] V. V. Kabanov, Electron-electron and electron-phonon relaxation in metals excited by optical pulse, *Low Temp. Phys.* **46**, 414 (2020).
- [6] C. Chen, Zh. Tao, A. Carr, P. Matyba, T. Szilvási, S. Emmerich, M. Piecuch, M. Keller, Dm. Zusin, St. Eich *et al.*, Distinguishing attosecond electron-electron scattering and screening in transition metals, *Proc. Natl Acad. Sci. USA* **114**, E5300 (2017).
- [7] E. Linardy, M. Trushin, K. Watanabe, T. Taniguchi, and G. Eda, Electro-optic upconversion in van der Waals heterostructures via nonequilibrium photocarrier tunneling, *Adv. Mater.* **32**, 2001543 (2020).
- [8] I.-J. Chen, S. Limpert, W. Metaferia, C. Thelander, L. Samuelson, F. Capasso, A. M. Burke, and H. Linke, Hot-carrier extraction in nanowire-nanoantenna photovoltaic devices, *Nano Lett.* **20**, 4064 (2020).
- [9] M.-B. Tran and Y. Pomeau, Boltzmann-type collision operators for Bogoliubov excitations of Bose-Einstein condensates: A unified framework, *Phys. Rev. E* **101**, 032119 (2020).
- [10] J.-P. Joost, N. Schlünzen, and M. Bonitz, G1-G2 scheme: Dramatic acceleration of nonequilibrium Green functions simulations within the Hartree-Fock generalized Kadanoff-Baym ansatz, *Phys. Rev. B* **101**, 245101 (2020).
- [11] A. E. Lukyanov, V. D. Neverov, Ya. V. Zhumagulov, A. P. Menushenkov, A. V. Krasavin, and A. Vagov, Laser-induced ultrafast insulator-metal transition in BaBiO<sub>3</sub>, *Phys. Rev. Res.* **2**, 043207 (2020).
- [12] R. Tuovinen, D. Golež, M. Eckstein and M. A. Sentef, Comparing the generalized Kadanoff-Baym ansatz with the full Kadanoff-Baym equations for an excitonic insulator out of equilibrium, *Phys. Rev. B* **102**, 115157 (2020).
- [13] M. Bonitz, *Quantum Kinetic Theory* (Springer International Publishing, Switzerland, Cham, 2016).
- [14] L. Borkowski, N. Schlünzen, J.-Ph. Joost, F. Reiser and M. Bonitz, Doublon production in correlated materials by multiple ion impacts, *Phys. Status Solidi B* **259**, 2100511 (2022).
- [15] G. D. Tsididis, L. Mouchliadis, M. Pedio, and E. Stratakis, Modeling ultrafast out-of-equilibrium carrier dynamics and relaxation processes upon irradiation of hexagonal silicon carbide with femtosecond laser pulses, *Phys. Rev. B* **101**, 075207 (2020).
- [16] T. M. Mishonov, G. V. Pachov, I. N. Genchev, L. A. Atanasova, and D. Ch. Damianov, Kinetics and Boltzmann kinetic equation for fluctuation Cooper pairs, *Phys. Rev. B* **68**, 054525 (2003).
- [17] H. Haug, A.-P. Jauho, Transport in Mesoscopic Semiconductor structures, in *Quantum Kinetics in Transport and Optics of Semiconductors*, Solid-State Sciences, Vol. 123 (Springer, Berlin, Heidelberg, 2008).
- [18] J. Singh, *Electronic and Optoelectronic Properties of Semiconductor Structures* (Cambridge University Press, Cambridge, 2003).
- [19] V. V. Kabanov and A. S. Alexandrov, Electron relaxation in metals: Theory and exact analytical solutions, *Phys. Rev. B* **78**, 174514 (2008).
- [20] M. Wais, M. Eckstein, R. Fischer, P. Werner, M. Battiato, and K. Held, Quantum Boltzmann equation for strongly correlated systems: Comparison to dynamical mean field theory, *Phys. Rev. B* **98**, 134312 (2018).
- [21] F. Caruso and D. Novko, Ultrafast dynamics of electrons and phonons: from the two-temperature model to the

- time-dependent Boltzmann equation, *Adv. Phys.: X* **7**, 2095925 (2022).
- [22] B. Rethfeld, A. Kaiser, M. Vicanek and G. Simon, Ultrafast dynamics of nonequilibrium electrons in metals under femtosecond laser irradiation, *Phys. Rev. B* **65**, 214303 (2002).
- [23] Yu. N. Ovchinnikov and V. Z. Kresin, Nonstationary state of superconductors: Application to nonequilibrium tunneling detectors, *Phys. Rev. B* **58**, 12416 (1998).
- [24] V. V. Kabanov, J. Demsar, and D. Mihailovic, Kinetics of a Superconductor Excited with a Femtosecond Optical Pulse, *Phys. Rev. Lett.* **95**, 147002 (2005).
- [25] A. Rothwarf and B. N. Taylor, Measurement of Recombination Lifetimes in Superconductors, *Phys. Rev. Lett.* **19**, 27 (1967).
- [26] J. Demsar, Non-equilibrium phenomena in superconductors probed by femtosecond time-domain spectroscopy, *J. Low Temp. Phys.* **201**, 676 (2020).
- [27] I. Avigo, R. Cortés, L. Rettig, S. Thirupathaiah, H. S. Jeevan, P. Gegenwart, T. Wolf, M. Ligges, M. Wolf, J. Fink *et al.*, Coherent excitations and electron-phonon coupling in Ba/EuFe<sub>2</sub>As<sub>2</sub> compounds investigated by femtosecond time- and angle-resolved photoemission spectroscopy, *J. Phys.: Condens. Matter* **25**, 094003 (2013).
- [28] P. F. Kartsev, Effective simulation of kinetic equations for bosonic system with two-particle interaction using OpenCL, in *Proceedings of IWOCL 2017: the 5th International Workshop on OpenCL* (Association for Computing Machinery, New York, 2017), paper 28.
- [29] <https://github.com/pkartsev/flbe>.
- [30] A. Alekseenko and J. Limbacher, Evaluating high order discontinuous Galerkin discretization of the Boltzmann collision integral in  $O(N^2)$  operations using the discrete Fourier transform, [arXiv:1801.05892](https://arxiv.org/abs/1801.05892).
- [31] S. W. Smith, *The Scientist and Engineer's Guide to Digital Signal Processing*, 2nd ed. (California Technical Publishing, San Diego, 1999), p. 118.
- [32] H. S. Köhler, Memory and correlation effects in the quantum theory of thermalization, *Phys. Rev. E* **53**, 3145 (1996)
- [33] R. Binder, H. S. Köhler, M. Bonitz, and N. Kwong, Green's function description of momentum-orientation relaxation of photoexcited electron plasmas in semiconductors, *Phys. Rev. B* **55**, 5110 (1997)
- [34] M. Bonitz, D. Kremp, D. C. Scott, R. Binder, W.-D. Kraeft, H. S. Köhler, Numerical analysis of non-Markovian effects in charge-carrier scattering: one-time versus two-time kinetic equations, *J. Phys.: Condens. Matter* **8**, 6057 (1996)
- [35] T. Ando, A. B. Fowler, and F. Stern, Electronic properties of two-dimensional systems, *Rev. Mod. Phys.* **54**, 437 (1982).
- [36] I. Mili, H. Latelli, Z. Charifi, H. Baaziz, T. Ghellab, A simple formula for calculating the carrier relaxation time, *Comput. Mater. Sci.* **213**, 111678 (2022).
- [37] J. Amarel, D. Belitz, and T. R. Kirkpatrick, Exact solution of the Boltzmann equation for low-temperature transport coefficients in metals. I. Scattering by phonons, antiferromagnons, and helimagnons, *Phys. Rev. B* **102**, 214306 (2020).
- [38] M. X. Na, F. Boschini, A. K. Mills, M. Michiardi, R. P. Day, B. Zwartsenberg, G. Levy, S. Zhdanovich, A. F. Kemper, D. J. Jones, and A. Damascelli, Establishing nonthermal regimes in pump-probe electron relaxation dynamics, *Phys. Rev. B* **102**, 184307 (2020).
- [39] B. J. DeSalvo, K. Patel, J. Johansen, and Ch. Chin, Observation of a Degenerate Fermi Gas Trapped by a Bose-Einstein Condensate, *Phys. Rev. Lett.* **119**, 233401 (2017).
- [40] C. Ravensbergen, V. Corre, E. Soave, M. Kreyer, E. Kirilov, and R. Grimm, Production of a degenerate Fermi-Fermi mixture of dysprosium and potassium atoms, *Phys. Rev. A* **98**, 063624 (2018).
- [41] A. Mosk, S. Kraft, M. Mudrich, K. Singer, W. Wohlleben, R. Grimm, and M. Weidemüller, Mixture of ultracold lithium and cesium atoms in an optical dipole trap, *Appl. Phys. B* **73**, 791-799 (2001)
- [42] K. E. Wilson, A. Guttridge, J. Segal, and S. L. Cornish, Quantum degenerate mixtures of Cs and Yb, *Phys. Rev. A* **103**, 033306 (2021).
- [43] M. Mudrich, S. Kraft, K. Singer, R. Grimm, A. Mosk, and M. Weidemüller, Sympathetic Cooling with Two Atomic Species in an Optical Trap, *Phys. Rev. Lett.* **88**, 253001 (2002).
- [44] M. Anderlini, E. Courtade, M. Cristiani, D. Cossart, D. Ciampini, C. Sias, O. Morsch, and E. Arimondo, Sympathetic cooling and collisional properties of a Rb-Cs mixture, *Phys. Rev. A* **71**, 061401(R) (2005).
- [45] M. Taglieber, A.-C. Voigt, T. Aoki, T. W. Hänsch, and K. Dieckmann, Quantum Degenerate Two-Species Fermi-Fermi Mixture Coexisting with a Bose-Einstein Condensate, *Phys. Rev. Lett.* **100**, 010401 (2008).
- [46] G. Delannoy, S. G. Murdoch, V. Boyer, V. Josse, P. Bouyer, and A. Aspect, Understanding the production of dual Bose-Einstein condensation with sympathetic cooling, *Phys. Rev. A* **63**, 051602(R) (2001).
- [47] M. Wais, K. Held, and M. Battiato, Numerical solver for the time-dependent far-from-equilibrium Boltzmann equation, *Comput. Phys. Commun.* **264**, 107877 (2021).
- [48] S. Trotzky, Y.-A. Chen, A. Flesch, I. P. McCulloch, U. Schollwöck, J. Eisert, and I. Bloch, Probing the relaxation towards equilibrium in an isolated strongly correlated one-dimensional Bose gas, *Nat. Phys.* **8**, 325 (2012).
- [49] M. P. Telenkov, Yu. A. Mityagin, V. V. Agafonov, and K. K. Nagaraja, Mechanism of energy relaxation in the system of Landau levels in quantum wells, *JETP Lett.* **102**, 678 (2015).
- [50] P. F. Kartsev and I. O. Kuznetsov, Effect of transport current on suppression of superconductivity with ultrashort laser pulse, *J. Phys.: Condens. Matter* **33**, 295601 (2021).